



A Journal of the Gesellschaft Deutscher Chemiker

# Angewandte Chemie

GDCh

International Edition

www.angewandte.org

## Accepted Article

**Title:** A Microporous Covalent Organic Framework with Abundant Accessible Carbonyls for Lithium-Ion Batteries

**Authors:** Zhiqiang Luo, Luoja Liu, Jiaxin Ning, Kaixiang Lei, Yong Lu, Fujun Li, and Jun Chen

This manuscript has been accepted after peer review and appears as an Accepted Article online prior to editing, proofing, and formal publication of the final Version of Record (VoR). This work is currently citable by using the Digital Object Identifier (DOI) given below. The VoR will be published online in Early View as soon as possible and may be different to this Accepted Article as a result of editing. Readers should obtain the VoR from the journal website shown below when it is published to ensure accuracy of information. The authors are responsible for the content of this Accepted Article.

**To be cited as:** *Angew. Chem. Int. Ed.* 10.1002/anie.201805540  
*Angew. Chem.* 10.1002/ange.201805540

**Link to VoR:** <http://dx.doi.org/10.1002/anie.201805540>  
<http://dx.doi.org/10.1002/ange.201805540>

## A Microporous Covalent Organic Framework with Abundant Accessible Carbonyls for Lithium-ion Batteries

Zhiqiang Luo, Luojia Liu, Jiaxin Ning, Kaixiang Lei, Yong Lu, Fujun Li\*, and Jun Chen

**Abstract:** A key challenge faced by organic electrodes is how to promote the redox reactions of functional groups to achieve high specific capacity and rate performance. Here, we report a two-dimensional (2D) microporous covalent organic framework (COF), poly(imide-benzoquinone), via in-situ polymerization on graphene (PIBN-G) to function as a cathode material for lithium-ion batteries (LIBs). Such a structure favors charge transfer from graphene to PIBN and full access of both electrons and  $\text{Li}^+$  to the abundant redox-active carbonyls, which are essential for battery reactions. This enables large reversible specific capacities of 271.0 and 193.1  $\text{mAh g}^{-1}$  at 0.1 and 10C, respectively, and retention of >86% after 300 cycles. The discharging/charging process successively involves  $8\text{Li}^+$  and  $2\text{Li}^+$  in carbonyls of the respective imide and quinone groups. The structural merits of PIBN-G will trigger more investigations into the designable and versatile COFs for electrochemistry.

Organic lithium-ion batteries (LIBs) are considered as one of the next-generation energy storage devices because of the tunable molecular structure, recyclability, and low cost of the organic electrode materials.<sup>[1,2]</sup> However, small organic molecules are plagued by their solubility in aprotic electrolytes and intrinsically low electric conductivity.<sup>[3,4]</sup> One efficient strategy is to stitch organic molecules to polymeric moieties and inhibit the dissolution.<sup>[5,6]</sup> This usually incurs agglomeration of polymer chains, and results in poor access of redox-active groups by  $\text{Li}^+$  or electrons, which are essential for electrochemical reactions, and hence low utilization efficiency of <70% of the polymers, especially at high rates.<sup>[7,8]</sup> Microporous polymers with two- or three-dimensional (2D or 3D) frameworks and controllable pore size favor permeation of aprotic electrolyte and diffusion of ions.<sup>[9-11]</sup> Structuring microporous polymer framework electrodes with both facile  $\text{Li}^+$  diffusion and electron transport is of crucial importance for organic LIBs.

Covalent organic frameworks (COFs) have attracted extensive interests in gas separation,<sup>[12]</sup> electrolyte membrane,<sup>[13]</sup> and electrochemical devices recently.<sup>[14,15]</sup> Rational design of COFs is effective to realize their versatile functionalities and applications. By tuning the functional groups, Jiang's group reported a COF from hexaazatrinaphthalene and diethynylbenzene to deliver a capacity of 147  $\text{mAh g}^{-1}$ .<sup>[15a]</sup> A thin film from naphthalene diimide and triformylphloroglucinol was obtained to improve  $\text{Li}^+$  diffusion and deliver 200  $\text{mAh g}^{-1}$  with conjugated carbonyls as redox centers.<sup>[15b]</sup> On the other hand, carbon nanotubes were incorporated into a donor-acceptor COF with a capacity of 69  $\text{mAh g}^{-1}$  at 2.4C; although its rate performance is improved, the achievable capacity is

compromised by the limited redox centers.<sup>[15c]</sup> COFs have been applied as electrode materials for LIBs,<sup>[16]</sup> but the electrochemical performance, like capacity, rate capability, and cycle stability, is still low and needs improvement. Appropriate design and synthesis of COFs with abundant accessible redox centers and electron conduction pathways are highly desirable for organic LIBs.

Herein, a microporous COF, poly(imide-benzoquinone), is synthesized from tetramino-benzoquinone (TABQ) and pyromellitic dianhydride (PMDA) with and without graphene (PIBN-G and PIBN). The as-synthesized PIBN is featured as a 2D framework with micropores of 1.5 nm, which facilitates diffusion and access of electrolyte to its abundant redox carbonyls. Favored by graphene, PIBN-G exhibits both good electron conduction and  $\text{Li}^+$  diffusion. These ensure full utilization of the carbonyls and hence a large capacity of 271  $\text{mAh g}^{-1}$  with fast kinetics and long cycle stability. It is revealed that the lithiation and delithiation processes of PIBN involve  $8\text{Li}^+$  and  $2\text{Li}^+$  in the carbonyls of the respective imide and quinone groups of each repeat unit of the COF in two successive steps. This will encourage more investigations into the designable and functional COFs.

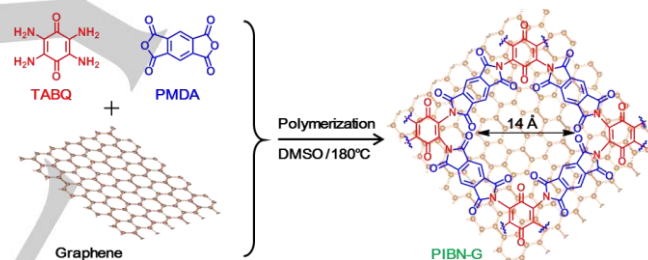


**Figure 1.** Synthesis route of PIBN and PIBN-G.

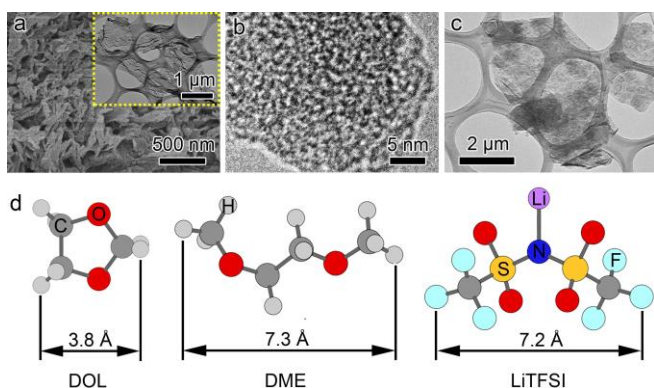
PIBN and PIBN-G were synthesized via a solvothermal reaction of TABQ and PMDA in dimethyl sulfoxide (DMSO) at 180 °C with and without addition of graphene, as depicted in Figure 1. The experimental details can be found in Supporting Information and Scheme S1 and S2. The obtained samples were characterized by both liquid  $^1\text{H}$  and solid-state  $^{13}\text{C}$  nuclear magnetic resonance (NMR) spectroscopy (Figure S1), elemental analysis (Table S1), and Fourier-transform infrared spectroscopy (FTIR, Figure S2). The average molecular weight of PIBN is 8052 (Figure S3). These indicate formation of PIBN of high purity. The content of graphene with ~7 layers (Figure S4) in PIBN-G is estimated to be 20 wt%, according to thermogravimetric analysis (Figure S5).

Figure 2a shows a typical scanning electron microscope (SEM) image of PIBN as well as Figure S6, in which it is agglomerated as nanoflakes. The layer structure of PIBN is evident in the transmission electron microscope (TEM) image in the inset of Figure 2a. The stacking multiple layers of PIBN can be seen from the high-resolution TEM image in Figure S7. Of note, the micropores of ~1.5 nm are visible in PIBN in Figure 2b, which is consistent with its molecular framework structure in Figure 1 and pore-size distribution from  $\text{N}_2$  sorption isotherms in Figure S8. With addition of graphene, PIBN-G appears as thin crystalline

[\*] Z. Luo, L. Liu, J. Ning, K. Lei, Y. Lu, Prof. F. Li, Prof. J. Chen  
Key Laboratory of Advanced Energy Materials Chemistry (Ministry of Education), College of Chemistry, Nankai University, Tianjin 300071, China  
E-mail: fujunli@nankai.edu.cn

Supporting information for this article is given via a link at the end of the document.

nanosheets in Figure 2c, Figure S9 and S10. The molecule sizes of DOL (1,3-dioxolane), DME (dimethoxyethane), and LiTFSI (lithium bis(trifluoromethanesulfonyl)imide) are calculated to be 0.38, and 0.73 nm, 0.72, respectively, in Figure 2d, which are the electrolyte components. It means that the electrolyte can facilitate transport in the micropores of  $\sim 1.5$  nm, as displayed in Figure 1 and 2b, and fully access the abundant redox carbonyls of PIBN.



**Figure 2.** (a) SEM image with an inset of TEM image and (b) High-resolution TEM image of PIBN, (c) TEM image of PIBN-G, and (d) Optimized geometries of DOL, DME, and LiTFSI.

Raman spectrum of PIBN-G is shown with PIBN and graphene in Figure 3a. The pure PIBN presents two Raman bands at 1344 and 1538  $\text{cm}^{-1}$ , respectively, which are assigned to the  $\text{sp}^2$  hybridization of C in phenyl groups and similar to the D and G bands of graphene at  $\sim 1320$  and 1580  $\text{cm}^{-1}$ .<sup>[17]</sup> The intensity ratio of the D and G bands of PIBN-G is increased to 1.45 from 0.38 of graphene, and its G band is positively shifted. This indicates existence of strong interaction between PIBN and graphene in PIBN-G. Charge differential density of PIBN-G from density functional theory (DFT) calculations is depicted in Figure 3b, where charge re-distribution exists between the PIBN molecule and graphene. The blue regions on graphene and yellow regions on PIBN indicate charge transfer from graphene to PIBN via conjugation of  $\pi$ - $\pi$  stacking,<sup>[18]</sup> which enhances the stability of PIBN molecules and promotes electron conduction of PIBN-G. Furthermore, X-ray photoelectron spectroscopy (XPS) spectra of PIBN-G, PIBN, and graphene are displayed in Figure 3c and d. Their elemental compositions are exhibited in wide-scan XPS spectra in Figure S11. In the N1s spectra of Figure 3c, the N-C peak of PIBN-G shifts to lower binding energy, implying  $\pi$ - $\pi$  stacking and electron transfer between the phenyl groups of PIBN and six-member carbon rings of graphene. This is in good agreement with the DFT calculations in Figure 3b and Figure S12. The emergence of  $\pi$ - $\pi^*$  satellite peak in Figure 3d further confirms that PIBN molecules are strongly interacting with graphene in PIBN-G.

The as-synthesized PIBN-G and PIBN are studied as cathode materials of LIBs in coin cells. The applied electrolyte is 1.0 M of LiTFSI in DOL and DME (v.v, 1:1). Figure 4a shows the electrochemical impedance spectroscopy (EIS) of PIBN-G and PIBN. The semicircles in high frequency regions denote charge transfer resistance ( $R_{ct}$ ), which is related to reaction kinetics, and the straight line in low frequency regions represents  $\text{Li}^+$  diffusion resistance in the electrolyte. It is clear that  $R_{ct}$  of PIBN-G is much smaller than that of PIBN (169.4 v.s. 280.2  $\Omega$ ), suggesting faster reaction kinetics of PIBN-G. Cyclic voltammetry (CV) curves of PIBN and PIBN-G are obtained at 0.5  $\text{mV s}^{-1}$  in Figure 4b. The two distinctive couples of redox peaks are ascribed to

their two successive lithiation/delithiation steps. The peak voltage differences of the two redox couples of PIBN-G are smaller than those of PIBN, and the peak areas of the two redox couples are larger than those of PIBN. These suggest lower polarization and higher utilization of redox carbonyls in PIBN-G than in PIBN. This is consistent with the lower charge transfer resistance of PIBN-G, as indicated by EIS in Figure 4a.

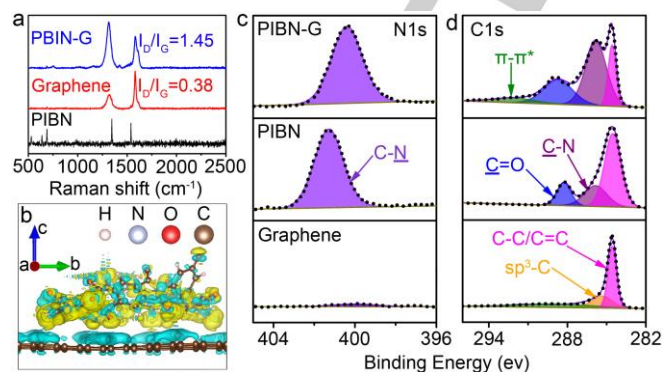


**Figure 3.** (a) Raman spectra of PIBN, graphene, and PIBN-G, (b) Simulated differential charge density of PIBN-G, and (c,d) XPS spectra of N1s and C1s.

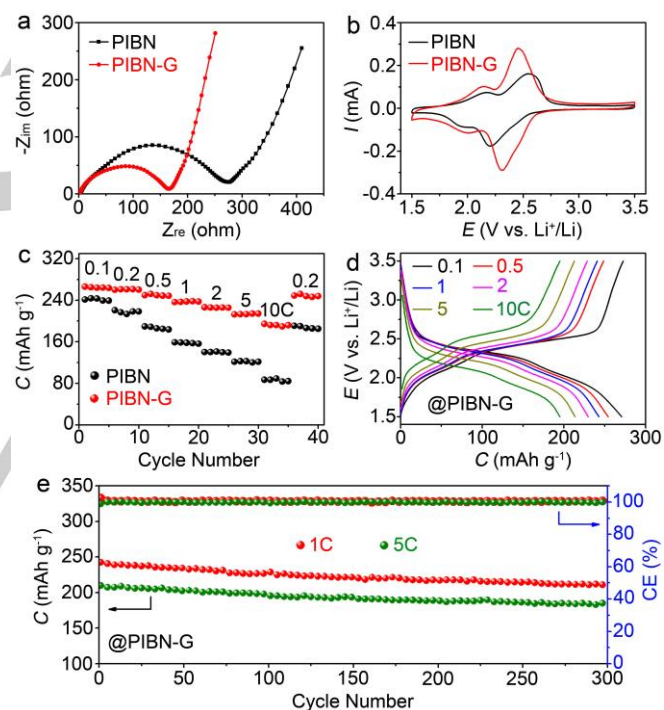


**Figure 4.** (a) EIS, (b) CV curves at 0.5  $\text{mV s}^{-1}$ , and (c) Rate performance of PIBN-G and PIBN, and (d) Discharge/charge profiles and (e) Cycle stability of PIBN-G. The current and capacity are based on the mass of PIBN.

The discharge capacities of PIBN-G are obtained at varied current rates of 0.1, 0.2, 0.5, 1, 2, 5, and 10C, together with PIBN in Figure 4c. At 0.1C, a high discharge capacity of 271.0  $\text{mAh g}^{-1}$  (601  $\text{Wh kg}^{-1}$ ) is achieved at PIBN-G, which is close to the theoretical value of 280.0  $\text{mAh g}^{-1}$  and corresponds to a utilization of 96.8%. At the same condition, the specific capacity of PIBN is only 244.8  $\text{mAh g}^{-1}$ , leading to a lower utilization of 86.1%. It is more evident to obtain larger specific capacities on PIBN-G over PIBN at high rates in Figure 4c. This is favored by the fast  $\text{Li}^+$  and electron transport in PIBN-G, which is rewarded by the strong interaction and charge transfer between PIBN and graphene. Figure 4d presents the discharge/charge curves of

PIBN-G at different rates. They are composed of two distinctive discharge/charge plateaus, which suggest two successive lithiation/delithiation steps and are in good agreement with the two couples of redox peaks in the CV curves in Figure 4b. Moreover, the operando EIS of PIBN-G and PIBN during 100 cycles are recorded and summarized in Figure S13. The impedance of PIBN-G is gradually increased in initial cycles and becomes stable beyond 10 cycles, while in PIBN it is increasing with cycles. The cycle stability is also revealed by almost the same SEM image of in Figure S14,  $^1\text{H}$  NMR spectra, FTIR spectra in Figure S15, and Figure S16 during cycles, respectively. In Figure 4e, the PIBN-G delivers initial capacities of 242.3 and 206.7  $\text{mAh g}^{-1}$  at 1 and 5C, respectively, and maintains at 208.1 and 182.3  $\text{mAh g}^{-1}$  after 300 cycles. The high specific capacity, capacity retention, and good rate capability of PIBN-G are attributed to the 2D microporous framework with abundant accessible carbonyls, and strong interaction between PIBN and graphene.

A typical discharge and charge profile of PIBN-G at 0.1C is displayed in Figure 5a. The discharging and charging processes are monitored by in-situ FTIR. The testing cell is home-made

and depicted in Figure S17. During the test, the PIBN-G cathode is closely contacted with an attenuated total reflection (ATR) crystal, the setup of which is depicted in Figure S18. The characteristic absorbance peaks of PIBN-G in two regions in Figure 5b are of interest: the light blue region represents the breathing vibration of the C=O bonds of imide groups at  $\sim 1720 \text{ cm}^{-1}$ , and the gray region is ascribed to the vibration of the C=O bonds of quinone groups at  $\sim 1570 \text{ cm}^{-1}$ .<sup>[1b]</sup> Both of the two kinds of carbonyls are the active redox centers. In a discharging process, the signals of the C=O bonds of imide groups at  $\sim 1720 \text{ cm}^{-1}$  become weak and almost disappear beyond the first plateau; after fully discharged to 1.5 V, the signals of the C=O bonds of quinone groups at  $\sim 1570 \text{ cm}^{-1}$  disappear in the following step. This indicates that in the discharging process the C=O bonds of imide and quinone groups are successively lithiated in two steps. In the charging process, the signals of the C=O bonds of the imide and quinone groups emerge gradually, which is the reverse of the discharging process. This is in good agreement with the two separate couples of redox peaks and the two distinctive plateaus of the discharge/charge profiles in Figure 4b and d, respectively.

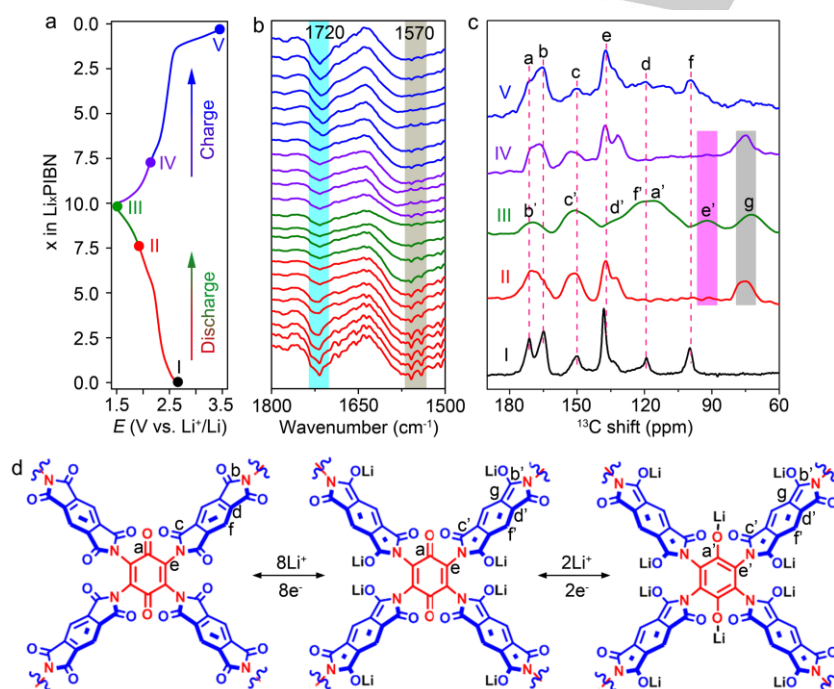


**Figure 5.** (a) Discharge/charge profile at 0.1 C, (b) In-situ FTIR spectra, (c) Ex-situ solid-state  $^{13}\text{C}$  NMR spectra collected at the indicated states in (a), and (d) Schematic gradual lithiation and delithiation of the different kinds of carbonyls of PIBN in a discharge and charge cycle.

The lithiation/delithiation of PIBN-G is further elucidated by solid-state  $^{13}\text{C}$  NMR, which is powerful to identify the different C=O bonds. Figure 5c presents the NMR spectra of PIBN-G at the selected discharged and charged states in Figure 5a. In the pristine Stage (I), PIBN shows six peaks at 171.7 (a) 165.1 (b), 150.4 (c), 118.9 (d), 138.5 (e), and 99.8 ppm (f), which are assigned to the various C atoms of PIBN, as marked in Figure 5d. When PIBN is discharged to 2.05 V at Stage (II), a new peak at 75.7 ppm (g) appears with disappearance of (d) and (f). It suggests lithiation of the C=O bonds of imide groups. In this step,  $8\text{Li}^+$  are inserted into PIBN, half of which are active for steric hindrance. At Stage (III) of full discharge, another new peak emerges at 92.0 ppm (e') with loss of (a) and (e), which indicates insertion of another  $2\text{Li}^+$  into the quinone groups in the second step. Upon subsequent charging, PIBN experiences a

reverse process at Stage (IV) and (V). It is believed that the lithiation/delithiation of PIBN occurs in two distinctive steps: the C=O bonds of imide groups are firstly inserted/extracted by  $8\text{Li}^+$  and then the C=O bonds of quinone groups accept/release another  $2\text{Li}^+$ . The reversible process is schematically depicted in Figure 5d.

In conclusion, we have successfully synthesized a microporous COF in the presence of graphene, PIBN-G. It is featured as a 2D framework with micropores of 1.5 nm. This favors diffusion and access of  $\text{Li}^+$  to the abundant redox carbonyls, and promotes the reversible electrochemical reactions. Rewarded by the strong interaction and charge transfer between PIBN and graphene, PIBN-G exhibits high electron conduction and  $\text{Li}^+$  diffusion, which benefit the redox reactions of carbonyls. It presents excellent rate capability with

large reversible capacities of 271.0 and 193.1 mAh g<sup>-1</sup> at 0.1 and 10C, respectively, and long cycle life of 300 cycles with Coulombic efficiencies of ~100%. The gradual lithiation and delithiation of PIBN-G involves 8Li<sup>+</sup> in the carbonyls of imide groups in the first step and another 2Li<sup>+</sup> in the carbonyls of quinone groups in the following step. Such high performance will trigger more investigations into the designable and versatile COFs for electrochemistry and promote the development of functional COFs.

## Acknowledgements

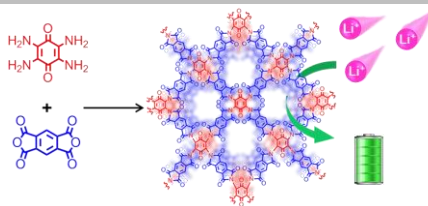
This work was supported by Ministry of Science and Technology (2016YFA0202503 and 2017YFA0206700), National Natural Science Foundation (51231003 and 21231005), and Ministry of Education of China (B12015).

**Keywords:** Lithium-ion batteries, organic cathode, covalent organic framework, carbonyl, micropores

- [1] a) M. Armand, J. M. Tarascon, *Nature* **2008**, *451*, 652-657; b) T. Ma, Q. Zhao, J. B. Wang, Z. Pan, J. Chen, *Angew. Chem. Int. Ed.* **2016**, *55*, 6428-6432; *Angew. Chem.* **2016**, *128*, 6538-6524.
- [2] a) H. Wang, S. Yuan, Z. Si, X. Zhang, *Energy Environ. Sci.* **2015**, *8*, 3160-3165; b) Z. Zhu, M. Hong, D. Guo, J. Shi, Z. Tao, J. Chen, *J. Am. Chem. Soc.* **2014**, *136*, 16461-16464.
- [3] a) Y. Liang, Z. Chen, Y. Jing, Y. Rong, A. Facchetti, Y. Yao, *J. Am. Chem. Soc.* **2015**, *137*, 4956-4959. b) T. Janoschka, N. Martin, U. Martin, C. Friebe, S. Morgenstern, H. Hiller, M. D. Hager, U. S. Schubert, *Nature* **2015**, *527*, 78-81.
- [4] a) Z. Luo, L. Liu, Q. Zhao, F. Li, J. Chen, *Angew. Chem. Int. Ed.* **2017**, *56*, 12561-12565; *Angew. Chem.* **2017**, *129*, 12735-12739; b) B. Genorio, K. Pirnat, R. Cerc-Korosec, R. Dominko, M. Gaberscek, *Angew. Chem. Int. Ed.* **2010**, *49*, 7222-7224; *Angew. Chem.* **2010**, *122*, 7380-7382.
- [5] Z. Song, Y. Qian, M. L. Gordin, D. Tang, T. Xu, M. Otani, H. Zhan, H. Zhou, D. Wang, *Angew. Chem. Int. Ed.* **2015**, *54*, 13947-13951; *Angew. Chem.* **2015**, *127*, 14153-14157.
- [6] S. Muench, A. Wild, C. Friebe, B. Haupler, T. Janoschka, U. S. Schubert, *Chem. Rev.* **2016**, *116*, 9438-9484.
- [7] Q. Zhao, Z. Zhu, J. Chen, *Adv. Mater.* **2017**, *29*, 1607007.
- [8] L. Gao, C. Y. V. Li, K. Y. Chan, Z. N. Chen, *J. Am. Chem. Soc.* **2014**, *136*, 7209-7212.
- [9] C. Sun, A. Klechikov, C. Moise, M. Prodana, M. Enachescu, A. V. Talyzin, *Angew. Chem. Int. Ed.* **2018**, *57*, 1034-1038; *Angew. Chem.* **2018**, *130*, 1046-1050.
- [10] Y. Zhang, J. Wang, S. N. Riduan, *J. Mater. Chem. A* **2016**, *4*, 14902-14914.
- [11] D. Chen, A. J. Avestro, Z. Chen, J. Sun, S. Wang, M. Xiao, Z. Erno, M. M. Algaradah, M. S. Nassar, K. Amine, Y. Meng, J. F. Stoddart, *Adv. Mater.* **2015**, *27*, 2907-2912.
- [12] C. Klumpen, M. Breunig, T. Homburg, N. Stock, J. Senker, *Chem. Mater.* **2016**, *28*, 5461-5470.
- [13] H. Chen, H. Tu, C. Hu, Y. Liu, D. Dong, Y. Sun, Y. Dai, S. Wang, H. Qian, Z. Lin, L. Chen, *J. Am. Chem. Soc.* **2018**, *140*, 896-899.
- [14] K. Sakaushi, G. Nickerl, F. M. Wisser, D. Nishio-Hamane, E. Hosono, H. S. Zhou, S. Kaskel, J. Eckert, *Angew. Chem. Int. Ed.* **2012**, *51*, 7850-7854; *Angew. Chem.* **2012**, *124*, 7972-7976.
- [15] a) F. Xu, X. Chen, Z. Tang, D. Wu, R. Fu, D. Jiang, *Chem. Commun.* **2014**, *50*, 4788-4790; b) C. R. DeBlase, K. Hernández-Burgos, J. M. Rotter, D. J. Fortman, D. dos S. Abreu, R. A. Timm, I. C. N. Diógenes, L. T. Kubota, H. D. Abruña, W. R. Dichtel, *Angew. Chem. Int. Ed.* **2015**, *54*, 13225-13229; *Angew. Chem.* **2015**, *127*, 13423-13427; c) F. Xu, S. Jin, H. Zhong, D. Wu, X. Yang, X. Chen, H. Wei, R. Fu, D. Jiang, *Sci. Rep.* **2015**, *5*, 8225-8231.
- [16] a) C. Zhang, X. Yang, W. Ren, Y. Wang, F. Su, J.-X. Jiang, *J. Power Sources* **2016**, *317*, 49-56; b) D.-H. Yang, Z.-Q. Yao, D. Wu, Y.-H. Zhang, Z. Zhou, X.-H. Bu, *J. Mater. Chem. A*, **2016**, *4*, 18621-18627.
- [17] H. Wang, P. Hu, J. Yang, G. Gong, L. Guo, X. Chen, *Adv. Mater.* **2015**, *27*, 2348-2354.
- [18] a) K. Momma, F. Izumi, *J. Appl. Cryst.* **2008**, *41*, 653-658; b) G. L. Gibson, T. M. McCormick, D. S. Seferos, *J. Am. Chem. Soc.* **2012**, *134*, 539-547.

## COMMUNICATION

A two-dimensional microporous covalent organic framework of poly(imide-benzoquinone) was synthesized via in-situ polymerization on graphene to function as a cathode material for lithium-ion batteries. It exhibits excellent electrochemical performance owing to the facile access of  $\text{Li}^+$  and electron to its abundant carbonyls.



Zhiqiang Luo, Luoja Liu, Jiaxin Ning, Kaixiang Lei, Yong Lu, Fujun Li\*, and Jun Chen

Page No. – Page No.

**A Microporous Covalent Organic Framework with Abundant Accessible Carbonyls for Lithium-Ion Batteries**

Accepted Manuscript